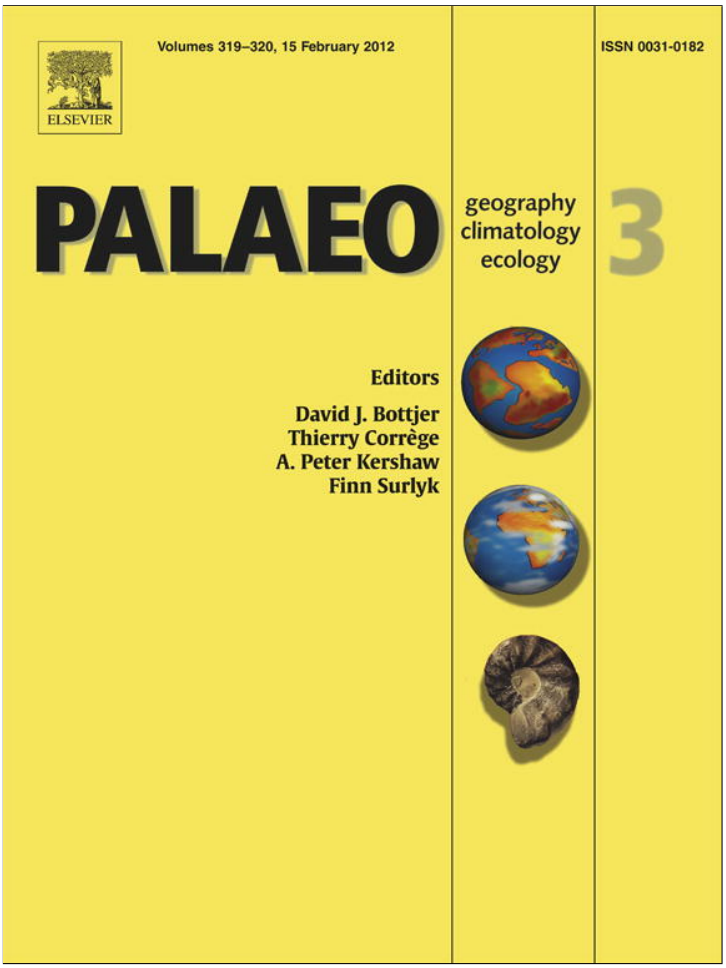

Palaeogeography, Palaeoclimatology, Palaeoecology 319-320 (2012) 93–106

Contents lists available at SciVerse ScienceDirect

Palaeogeography, Palaeoclimatology, Palaeoecology

journal homepage: www.elsevier.com/locate/palaeo

Speleothem deposition at the glaciation threshold — An attempt to constrain the age and paleoenvironmental significance of a detrital-rich flowstone sequence from Entrische Kirche Cave (Austria)

Michael C. Meyer [a,*], Christoph Spötl [a], Augusto Mangini [b], Richard Tessadri [c]

[a] Institut für Geologie und Paläontologie, Universität Innsbruck, Innsbruck, Austria
[b] Forschungsstelle Radiometrie, Heidelberger Akademie der Wissenschaften, Heidelberg, Germany
[c] Institut für Mineralogie und Petrographie, Universität Innsbruck, Innsbruck, Austria

ARTICLE INFO

Article history:
Received 15 December 2010
Received in revised form 12 December 2011
Accepted 3 January 2012
Available online 10 January 2012

Keywords:
Speleothems
Alps
Flowstone
Periglacial
Permafrost
Calcite fabric
Stadials
Interstadials
Last glacial cycle

ABSTRACT

Proxy records from high-altitude locations predating the Last Glacial Maximum are rare but could provide invaluable insights into the response of alpine catchments to the rapid climate fluctuations which characterized the last glacial period. Here we present a detrital-rich flowstone record from Entrische Kirche Cave, an inneralpine cave situated close to the accumulation area of the Pleistocene ice-stream network of the European Alps that expanded repeatedly into the lowlands during glacial maxima. U–Th dating of this calcite is challenging due to high detrital Th. However, petrographic and stable isotope analyses in conjunction with associated clastic cave sediments provide useful insights into the climatic boundary conditions during speleothem formation and into the paleoenvironmental processes which operated in the ~2000 m-high catchment above the cave.

Our data show that millennial-scale temperature fluctuations had a first-order control on the periglacial activity and vegetation in the catchment which strongly influenced the formation and infiltration of detritus into the karst aquifer. The brown laminated and brown dendritic fabrics that compose much of the detrital-rich flowstone succession reflect these environmental processes. The temperature-dependence of periglacial and permafrost processes allows to constrain the amount of cooling relative to the present-day mean annual air temperature that is required to initiate detrital-rich calcite formation in Entrische Kirche Cave, i.e. −2.5 °C (minimum) to −6 °C (maximum), respectively. White inclusion-poor calcite that is intercalated with the detrital-rich calcite indicates warm (interstadial) conditions and geomorphological stability in the catchment area. One such phase has been U–Th dated to 88.3 ± 6.9 ka (i.e. Greenland Interstadial 21 or 22).

1. Introduction

Reconstructing climate and paleoenvironmental change in (high) alpine environments is a challenging task because of the number and intensity of erosional processes that operate on such landscapes. A particularly well-studied example is the European Alps, where the repeated waxing and waning of ice-stream networks eroded most of the older paleoenvironmental archives during the Last Glacial Maximum (LGM; ca. 19–24 ka; Ivy-Ochs et al., 2008). As a consequence, archives in the Alps that pre-date the LGM are scarce and the detailed response of the alpine landscape to the complex succession of abrupt millennial-scale temperature fluctuations that characterised the middle and early parts of the last glacial cycle (i.e. the so-called Dansgaard–Oeschger (DO) events) remains largely elusive.

Speleothems allow us to gain "bottom-up" insights into the pre-LGM climate and paleoenvironmental evolution of the alpine realm. Protected from surface erosion speleothems can form continuously for many millennia and bear the great advantage of being precisely and accurately datable using U-series techniques (Henderson, 2006). Although formation of alpine speleothems preferentially occurs during warm interglacial and interstadial climatic conditions, speleothems also precipitate during cooler and less favourable climatic periods if the cave is situated in a low or intermediate altitude range, where cessation of calcite precipitation due to cave freezing occurs only during the most severe cold events (Holzkämper et al., 2005; Spötl et al., 2007).

For building U–Th chronologies using speleothems, clean calcite with low concentrations of detrital Th is preferable and in combination with stable oxygen isotope analysis the timing and duration of major isotope-defined climatic events can be constrained. This strategy results in atmospheric proxy signals ($\delta^{18}O$) that are accurately and precisely dated and can thus be supra-regionally correlated and compared (e.g. Wang, et al., 2008; Boch, et al., 2011). Cave calcites with a significant content of detrital material are usually avoided in speleothem studies, because of the need to correct for detrital ^{232}Th, which results in large age uncertainties (Richards and Dorale, 2003). Hence, limited research

* Corresponding author.
E-mail address: michael.meyer@uibk.ac.at (M.C. Meyer).

0031-0182/$ – see front matter © 2012 Elsevier B.V. All rights reserved.
doi:10.1016/j.palaeo.2012.01.010

on detrital-rich calcite from caves has been undertaken so far (e.g., Labonne, et al., 2002).

Detrital components in karst sediments comprise particles and colloids that are produced by the weathering of host rock and soil and are washed into the karst system. Such clastic sediments range in grain size from gravel to clay (Sasowsky and Mylroie, 2004; Palmer, 2007) and form metre-thick accumulations in many caves. Fine-grained detritus can be transported by seepage flow and become incorporated into speleothems. Such detrital phases can be present in speleothems as macroscopically visible silt or mud layers (Niggemann et al., 2003; Jaillet et al., 2006) or, more common, as microscopic particles concentrated in individual layers of calcite (Railsback et al., 1999). In addition, the presence of detritus can also be reflected by a change in the calcite fabric (Ayalon et al., 1999; Turgeon and Lundberg, 2001) and by certain trace elements commonly bound to detrital particles and/or colloids, e.g. Fe, Mn, Zn, Th, and Rare Earth Elements (e.g. Ayalon et al., 1999; Zhou et al., 2008; Fairchild and Treble, 2009).

Recent studies demonstrate the potential of detrital proxies and sediments for paleoclimate and paleoenvironmental research and suggest that they can (i) provide insights into Earth-surface processes that operated in the infiltration area during the time of speleothem formation (in contrast to speleothem $\delta^{18}O$ records that primarily reflect atmospheric processes (Goede et al., 1998; Frumkin and Stein, 2004; Richter et al., 2004; Hu et al., 2005; Li et al., 2005; Zhou et al., 2008; Schimpf et al., 2011)), but (ii) can also improve our understanding of the paleohydrology (Niggemann et al., 2003; Jaillet et al., 2006; Forbes and Bestland, 2007; Sroubek et al., 2007).

In this study we describe a brown, detrital-rich flowstone sequence from the inneralpine Entrische Kirche Cave (hereafter abbreviated as EKC) that was deposited intermittently during the middle and early parts of the last glacial cycle (Fig. 1). This calcite sequence is remarkable because it reveals a distinct isotopic and petrographic signature suggestive of extreme environmental change in the high-alpine infiltration area during speleothem formation (i.e. the mean annual air temperature in the infiltration area was just high enough to maintain an ice-free catchment and liquid water in the karst aquifer). Here we explore depositional and paleoenvironmental models to explain the formation of this unusual calcite sequence.

2. Geologic and geomorphologic settings

EKC is situated in the central Austrian Alps in close proximity to some of the highest summits of the main crests of the orogen (e.g., Großglockner 3798 m, Sonnblick 3105 m, Fig. 1). The distance from the cave to the northern rim of the Alps is ca. 55 km. The host rock is composed of calcite mylonite (Klammkalk; Exner, 1979). The entrance to the cave system is in the flank of the steep Gastein valley at an elevation of 1040 m asl and from there the cave extends into easterly direction for ~270 m (Fig. 2A). The total length of the cave is 1.6 km and the passages (elliptical tunnels which alternate with partly collapsed halls) are arranged in two sub-horizontal levels that are connected via shafts (Fig. 2B; Klappacher, 1992). A perennial stream with a peak discharge of ca. 10 L/s drains the lower cave level.

The small catchment area of the cave (~3 km^2) reaches up to 2119 m in elevation and rock overburden above the presently explored cave network is thus ≥900 m. Conifer forests cover the valley slopes up to ~1800–1900 m (i.e. the altitude of the regional timberline today) and alpine mats and shrubs constitute the vegetation in the infiltration area directly above the cave (Fig. 2C). The intensively folded host rock also controls the morphology in the catchment area, where anticlines form the backbone of mountain ridges and synclines host high-alpine lakes. Two such lakes are directly situated above EKC (Paar lakes, at 1856 and 1949 m, respectively), and are surrounded by steep slopes (Figs. 2A and C). Tracer experiments demonstrated a direct connection between a ponor on the northern shore of one of the lakes and the cave stream in the lower level of EKC (transit time 1 to 3 days, horizontal distance 1.8 km; Ganahl, 1991).

3. Chemical and clastic cave sediments

EKC hosts active and fossil flowstones, stalagmites, stalactites and soda straws, as well as clastic sediments. The latter comprise fine-grained gravel, sand and abundant silt and clay, attaining a thickness of up to 1.6 m (Fig. 2B). Gravel and sand are only present in the lowermost cave level, close to the modern stream. Grey silt and clay are widespread also in the higher levels of the cave. These fine-grained sediments were probably deposited during the LGM when the alpine ice-stream network (reaching an elevation of ~2000–2100 m in the study area — van Husen,

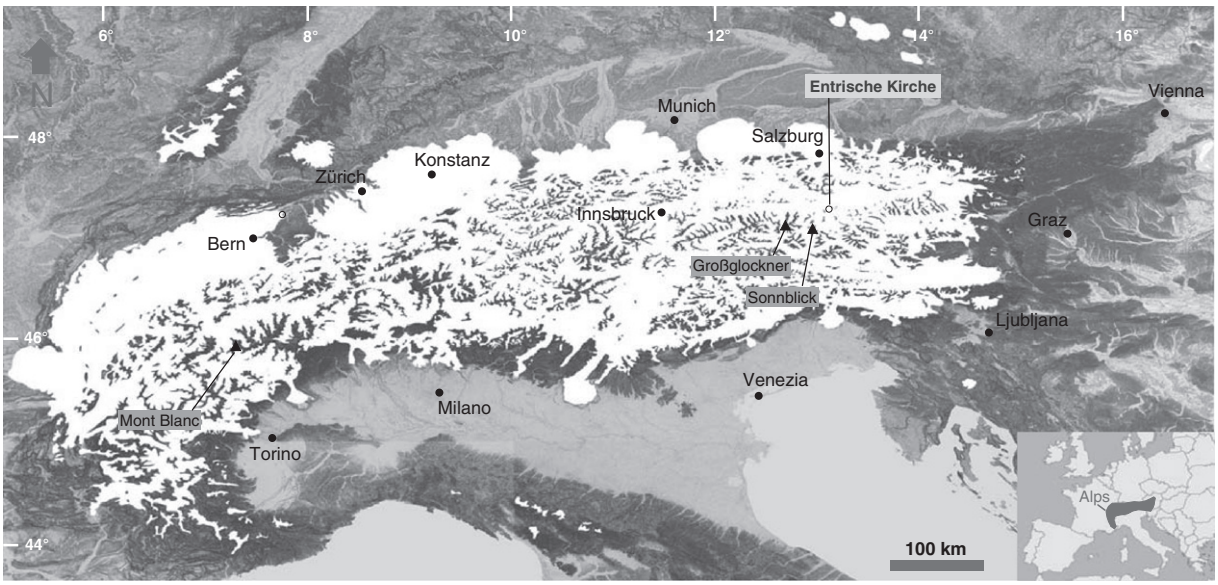

Fig. 1. The European Alps during the Last Glacial Maximum and position of the investigation area. Digital elevation model from Jarvis et al. (2008). Ice extent after Ehlers and Gibbard (2004).

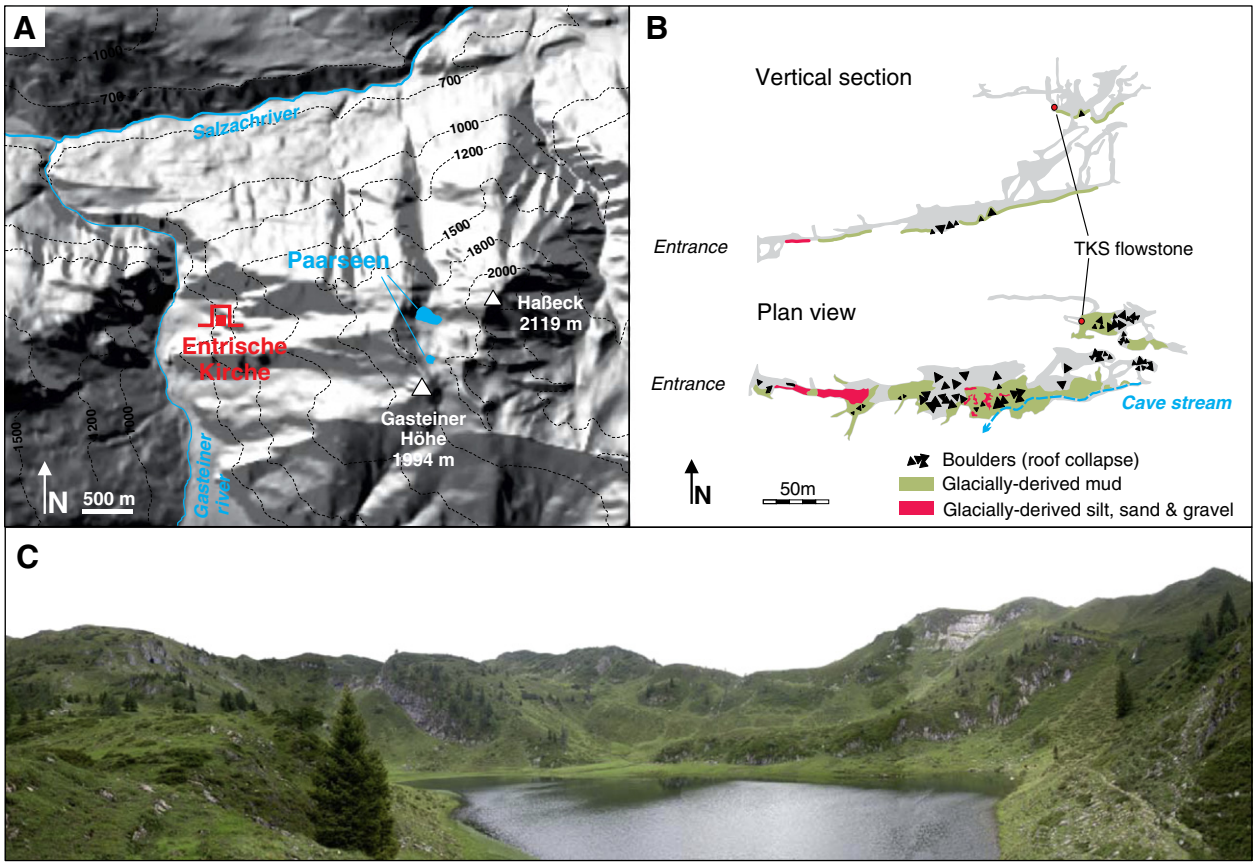

Fig. 2. Cave setting. A: Digital elevation model of the infiltration area of EKC. B: Cave plan. C: Panoramic view of the infiltration area of EKC (lower Paar lake, 1856 m asl).

1987) blocked the discharge from EKC and resulted in back-flooding of glacial meltwater. The timing is supported by two lines of evidence: (i) reworked fragments of cave bear bones within the coarser grained sediments yielded (uncalibrated) radiocarbon ages of 38.4 and 53.0 ka BP thus providing a maximum sedimentation age and (ii) speleothems resting on top of these sediments yielded early Holocene basal U–Th ages (i.e. constraining the minimum age of the sediments beneath (Table 1)).

U–Th dating on flowstones indicates repeated speleothem deposition during warm, interglacial periods, including Marine Isotope Stage (MIS) 7, 5 and 1, as well as during interglacial–glacial transitions (Meyer et al., 2008; Spötl, unpubl. data). Calcite precipitated during such interglacials is white, translucent or laminated and inclusion-poor and shows $\delta^{18}O$ values of ~−8 to −10‰. These values are close to the isotopic composition of actively forming flowstones (−10.2‰), which are precipitating under isotopic equilibrium today (Meyer et al., 2008).

The MIS 5e/d transition (i.e. the demise of the Eemian and the onset of the last glacial cycle) is recorded in several speleothems from EKC, most notably in samples from the TKS flowstone (Meyer et al., 2008). This flowstone is a large conical formation ~4 m in height, with a basal diameter of ~1.8 m and is situated at the base of a shaft in the upper cave level (Figs. 2B and 3). The flowstone is presently inactive and covered by medium-grey calcite. Four drill cores have been retrieved from this speleothem. U–Th dating revealed that white calcite was deposited between MIS 5e and the beginning of MIS 5d, followed by brown, detrital-rich calcite (Meyer et al., 2008; Fig. 4). A major drop in $\delta^{18}O$ by ~3‰, which took place at ca. 118 ka, is recorded in the white calcite sequence, demarcating the end of MIS 5e. Both, petrographic evidence and isotopic modelling suggest that strong seasonality changes were responsible for the observed shift in $\delta^{18}O$ and that the catchment area of EKC remained vegetated, geomorphologically stable and ice-free during the MIS 5e/d transition (Meyer et al., 2008). At ca. 114 ka, i.e. with the onset of stadial conditions and widespread ice-rafting in the North Atlantic, white calcite precipitation in EKC ceased (Meyer et al., 2008; Fig. 4). The brown detrital-rich calcite that follows up-section reveals a vastly different petrographic and isotopic signature.

Table 1
Radiocarbon ages on collagen extracted from reworked bones found in the clastic cave sediments in the lower cave level of EKC. AMS measurements made at the Leibniz-Laboratory for radiometric dating and isotope research. yrs. BP. — years before present.

Lab no.	% modern carbon (corr.)	^{14}C age (yrs. BP)	Error	$\delta^{13}C$ (‰)
EK1 KIA13963	0.84 ± 0.05	38,430	+480/−450	−22.42 ± 0.05
EK2 KIA13964	0.14 ± 0.04	53,030	+2510/−1910	−21.15 ± 0.27

4. Methods

A hand-held, battery-powered drill equipped with a diamond drill bit was used to obtain four long cores (2.5 cm diameter) from the TKS flowstone. Core samples were examined both macroscopically and in thin sections using transmitted-light and epifluorescence microscopy. Using a digital camera attached to the epifluorescence microscope a continuous transect of photomicrographs was retrieved along the entire brown calcite sequence of core TKS I for a detailed analysis of calcite growth, organic inclusions and microscopic corrosion features. Photomicrographs of selected laminated sequences, identified under the epifluorescence microscope, were processed using the WinGeol lamination tool (Meyer et al., 2006). Along a manually digitized lamina

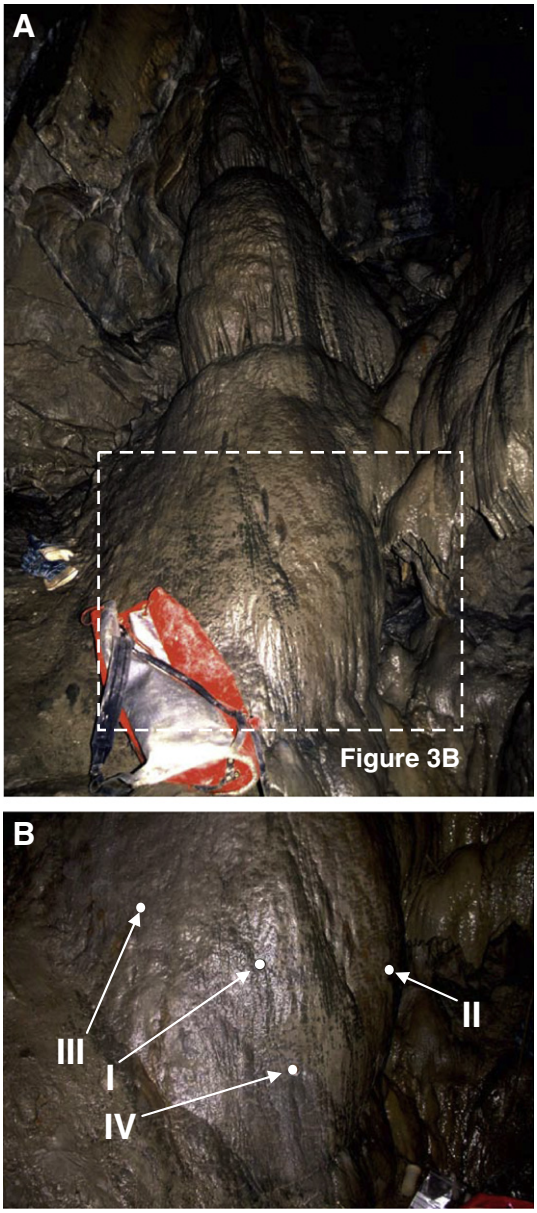

Fig. 3. The TKS (Teufelskrallen shaft) flowstone in the upper cave level. Caving bag for scale (77 cm in height); numbers in B indicate locations of the drill cores.

trace, thickness measurements of individual (fluorescent and non-fluorescent) calcite bands were performed and the combined thicknesses of the consecutive dark and bright fluorescent calcite couplets were calculated as well. Furthermore, the colour intensity of the epifluorescence images was obtained along each lamina trace (Meyer et al., 2006). Subsamples for stable carbon and oxygen isotope analyses were obtained at 0.2 mm increments with a Merchantek micromill for the cores TKS I, II and IV and analysed using a Thermofinnigan Delta^{Plus}XL mass spectrometer. Standardisation was accomplished by using the NBS19 standard, and results are reported relative to the Vienna Peedee Belemnite (VPDB) standard. The long-term 1σ precision of the $\delta^{13}C$ and $\delta^{18}O$ values (replicate analyses of a quality assurance standard) is 0.07 and 0.08‰, respectively. The elemental concentration of selected macroscopic calcite fabrics was determined using an energy-dispersive X-ray fluorescence analyser (ED-XRFA; model Spectro-XEPOS). The elemental concentration of Mg, Sr, Ba, Al, Si, Fe, Th and U for selected calcite fabrics was determined semi-quantitatively by placing sub-samples of the polished core with the respective calcite fabric directly below the XRF detector (detection limit ~10 ppm). Techniques used for U/Th preparation and TIMS analysis (using a Finnigan MAT 262 RPQ and the double filament technique) are detailed in Holzkämper et al. (2005). The calibration of the U and Th spikes is described in Hoffmann et al. (2007). Ages were calculated using the half lives by Cheng et al. (2000). Correction for detrital contamination assuming a $^{232}Th/^{238}U$ mass ratio equivalent to the average crust value (Richards and Dorale, 2003) and ^{230}Th and ^{234}U and ^{238}U in secular equilibrium for the detritus resulted in locally significant changes of the final ages.

5. Petrographic and isotopic characteristics of the brown calcite sequence

5.1. Macroscopic observations

Fig. 4 shows the topmost ~170 mm of the four TKS drill cores together with a schematic log of the petrography of core TKS I (our reference core for discussing the petrography and isotope data). Hiatus H1 (i.e. a major growth cessation at 114 ka; Meyer et al., 2008) separates the white inclusion-poor MIS 5d calcite from the brown detrital-rich sequence. A second hiatus (H2) is present within the brown detrital-rich calcite sequence at 59 mm. The total thickness of this brown detrital-rich calcite is ~100 mm in the cores TKS I, III and IV, but attains only ~70 mm in core TKS II. However, the internal succession of calcite units is the same for all four cores.

Both laminated and dendritic fabrics are present in the brown detrital-rich flowstone sequence (Fig. 4). The former is dense and individual laminae are typically 0.5–0.3 mm in thickness and are either light or medium brown in colour. Above ~18 mm brownish to greyish laminated calcite prevails and lamination becomes thin toward the top of the TKS cores (e.g. the lamina thickness is ≤0.25 mm between 0 and 4 mm of core TKS I). On a few occasions white, laminated and inclusion-poor calcite layers 1–4 mm in thickness are embedded into the brown laminated detrital-rich calcite sequence (i.e. at 68 mm and repeatedly in the topmost ~12 mm of core TKS I). The dendritic calcite (Frisia et al., 2000) is porous and reveals a light yellowish to brownish colour. Several dendritic calcite packages can be discerned and above hiatus H2 a thinning of the dendritic calcite packages up-section is observed. Furthermore, ~1 mm-thin, diffuse layers that reveal a dendritic fabric only under the microscope are intercalated in the brown laminated calcite (at least four such layers are present between 96 and 59 mm depth and labelled dendritic micro-layers in Figs. 4 and 5D).

5.2. Transmitted-light microscopy

The brownish and greyish laminated calcite shows a columnar fabric with individual crystals several mm to a few cm in length. Corrosion horizons can be observed occasionally under transmitted light (Fig. 5A). The major hiati H1 and H2 also show clear-cut corrosion features on the microscopic scale (Fig. 5A and B).

The brownish dendritic calcite is composed of branching polycrystals which are aligned sub-parallel to the growth axis of the TKS flowstone (Fig. 5A). Crystals usually start at nucleation points (e.g. at detritus-rich horizons) and are a few tens of micrometres thick and several hundred micrometres to locally a few millimetres in length. Under transmitted-light the colour of these bunches of calcite crystals is white translucent; some patches of this fabric, however, also reveal a light to medium brown colour.

5.3. Epifluorescence microscopy

The brown laminated calcite sequences reveal micron-scale lamination. UV-laminae are composed of fluorescent calcite bands (ca. 3–20 μm; termed fluorescent laminae; Fig. 6) and dark calcite bands lacking fluorescence (ca. 1–10 μm; termed non-fluorescent

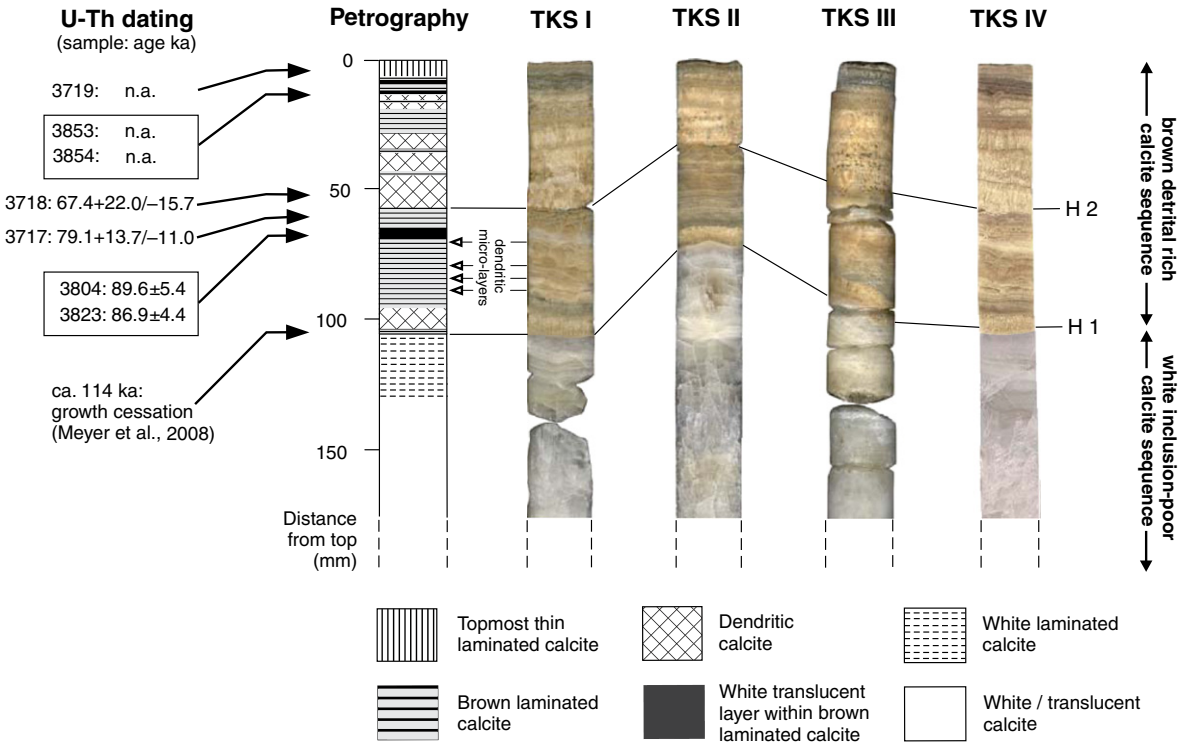

Fig. 4. Petrography of the TKS drill cores and U–Th ages (n.a. — not available).

laminae, Fig. 6). Fluorescent and non-fluorescent calcite bands form 2–30 μm thick lamina couplets (11 μm in average; Fig. 6). This type of fluorescent micro-banding is observed throughout the brown laminated calcite packages where it can form continuously laminated sequences up to several mm in thickness (Fig. 5C).

Corrosion horizons and micro-hiati are commonly observed using epifluorescence microscopy and at least 111 corrosion events were recognized in the brown laminated calcite between hiatus H1 and H2. Significant corrosion is also evident for the major hiati H1 and H2 (Fig. 5A and B).

No UV-lamination was found in the dendritic calcite units. Nevertheless, a diffuse but strong fluorescence is obvious under UV stimulation while the structure of the branching calcite crystals is still discernible (Fig. 5B and D). Dissolution appears much less common in the dendritic calcite fabric compared to the brown, laminated calcite packages.

The topmost 12 mm of the TKS cores (i.e. where macroscopic lamination starts to thin out and white laminae are intercalated) also reveal fluorescent micro-banding upon UV-stimulation. These UV-laminae, however, are rare and only short laminated sequences (<1 mm in length) are preserved. Corrosion horizons become prominent toward the top of the core and are regularly spaced (every ~100–200 μm; Fig. 5E).

5.4. Lamination analysis

Two sequences with continuous UV-lamination from the brown laminated calcite package below hiatus H2 of core TKS I were chosen for lamination analysis. Lamina track 1 (3 mm in length) extends from 58.8 to 61.8 mm (Fig. 6), while lamina track 2 (1.5 mm in length) covers the distance from 76.8 to 78.3 mm (not shown). The former lamina track encompasses 213 lamina couplets (5–30 μm in thickness), while the latter is composed of 166 such couplets (3–20 μm in thickness). The non-fluorescent bands are always slightly thinner and less variable compared to the fluorescent bands. Co-variation of lamina thicknesses of the non-fluorescent and the fluorescent bands exists (correlation coefficients of $r^2 = 0.25$ and $r^2 = 0.38$ for lamina track 1 and 2, respectively; Fig. 6). In both lamina tracks the greyscale curve varies between values of 40 and 110 (0 = black, 255 = white), indicating that the abundance of fluorescent substances in the speleothem calcite fluctuated significantly through time. The r^2 value indicates no correlation between the greyscale profile and lamina thicknesses (neither for the fluorescent bands: $r^2 \leq 0.09$; nor for the non-fluorescent bands: $r^2 \leq 0.06$; nor for the lamina couplets: $r^2 \leq 0.1$; Fig. 6).

5.5. Stable isotopes

All cores show the same isotopic trends and start with $\delta^{18}O$ values of ~−10.8 to −11‰ above hiatus H1 (Fig. 7B). At 96 mm (core TKS I) the $\delta^{18}O$ values decrease abruptly by ~0.8‰ and attain a minimum of −12‰ at 91.8 mm. From there $\delta^{18}O$ values increase steadily over the next 36 mm and reach $\delta^{18}O$ values of −11.2‰ just prior to hiatus H2 (59 mm). An abrupt isotopic jump is associated with hiatus H2 and $\delta^{18}O$ values of ~−10.2‰ are attained between H2 and 47 mm (i.e. the highest $\delta^{18}O$ values of the entire brown detrital-rich calcite sequence). Further up-section the $\delta^{18}O$ record of all TKS cores shows an overall decreasing trend. The topmost 4 mm of all cores are characterised by an irregular, high-amplitude, high-frequency isotope signal with $\delta^{18}O$ values fluctuating by more than 2‰.

The $\delta^{13}C$ record is characterised by a high-amplitude, high-frequency signal with $\delta^{13}C$ values that are – on average – increasing. The character of this $\delta^{13}C$ signal is remarkably similar between the TKS cores (Fig. 7A). $\delta^{13}C$ minima reach values as low as −8‰ between hiati H1 and H2 and −4‰ between hiatus H2 and the top of the cores. Positive excursions typically reach 1–2‰ but attain 4% in the topmost 4 mm of the flowstone.

Correlation coefficients between the $\delta^{13}C$ and $\delta^{18}O$ records were calculated for each calcite fabric separately (i.e. dendritic, laminated and thinly laminated calcite in the topmost ~4 mm of each core; Fig. 7C). The $\Delta\delta^{13}C/\Delta\delta^{18}O$ slope for each calcite fabric is always

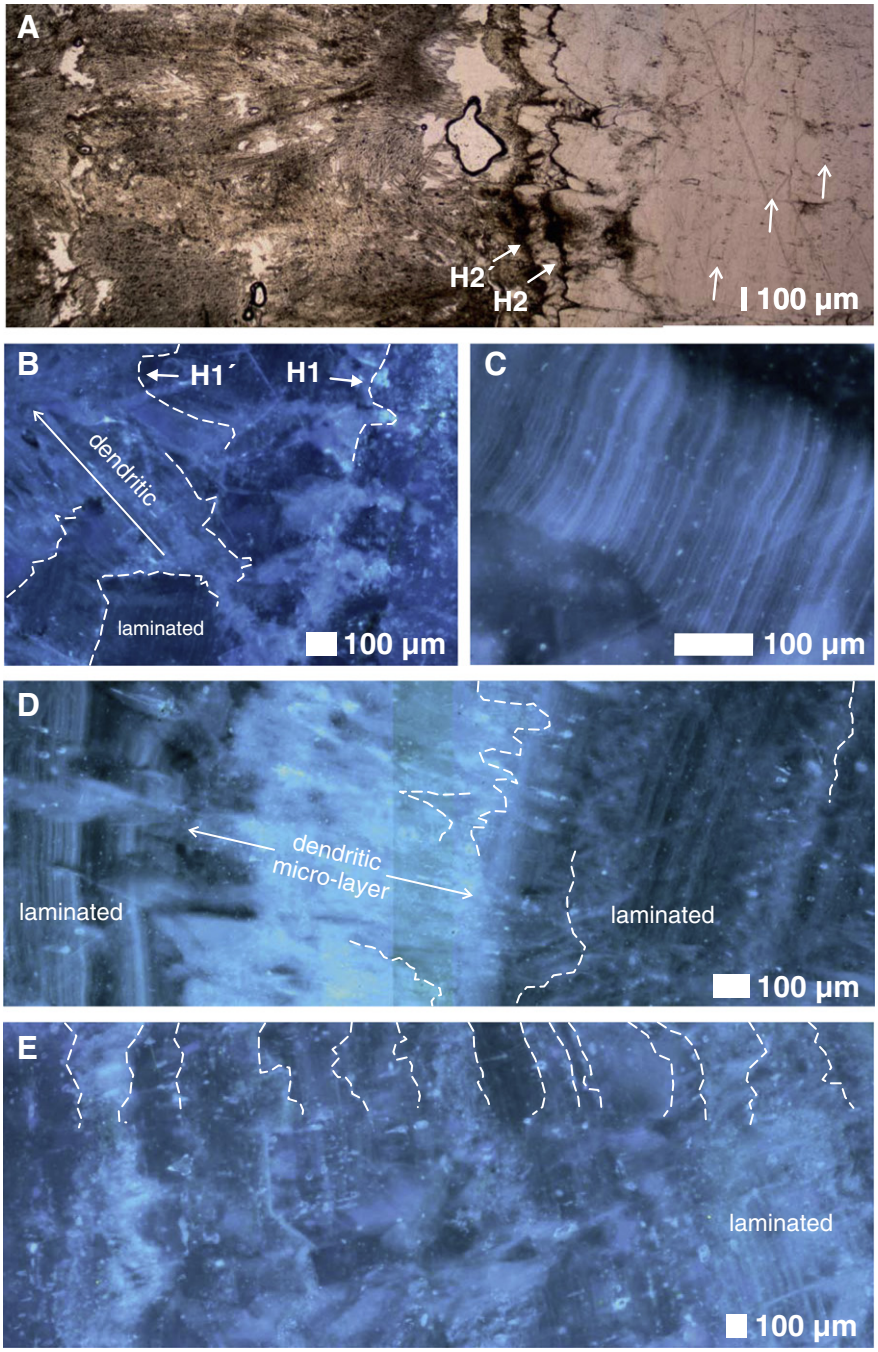

Fig. 5. Photomicrographs of the brown, detrital-rich calcite sequence. Top of flowstone always to the left; distances refer to depths in core TKS I (Fig. 4). A: Transmitted-light microscopy; hiatus H2 at ~59 mm. Note dendritic calcite with branching polycrystals above H2 and inclusion-rich layers (arrows) in the brown laminated calcite below H2. B–E: Epifluorescence microscopy. B: Hiatus H1 and the transition from the white inclusion-poor MIS 5d calcite into the brown, detrital-rich calcite. Remnants of brown laminated calcite which reveals micron-scale lamination are preserved at the base of the brown calcite sequence. Corrosion (broken lines) dissolved this laminated calcite almost entirely before dendritic calcite growth commenced (arrow). C: Example of regular fluorescent calcite banding (at ~77.2 mm i.e. in the macroscopically brown laminated calcite sequence). Note absence of corrosion features. D: Example of a dendritic micro-layer (i.e. ~1 mm thick dendritic, fluorescent band intercalated into the brown laminated calcite sequence). Corrosion features highlighted by broken lines. 68–70.5 mm depth. E: Near the top of core TKS I (~4–6 mm) the UV-lamination is faint and non-fluorescent calcite bands (forming the macroscopically white calcite layers) are dominant. Note frequent and regularly spaced corrosion horizons (broken lines).

positive and steep (i.e. between 1.2 and 5.6), whereas the r^2 values vary considerably i.e. r^2 values are low for the laminated calcite (0.02–0.08), high for the dendritic calcite fabric (0.46–0.52) and intermediate in the topmost part of the TKS cores (0.14–0.33; Fig. 7C). Furthermore, large variation in the $\delta^{13}C$ (>6‰) contrasts with rather small changes in $\delta^{18}O$ (typically ~1‰) in all cores. Finally, dendritic calcite is isotopically always distinct from the laminated calcite (showing slightly higher $\delta^{18}O$ and $\delta^{13}C$ values), although both calcite fabrics partly overlap in their $\delta^{13}C$ vs. $\delta^{18}O$ values (Fig. 7C).

There is also a clear relationship between isotopic composition and petrography in these flowstone samples: dendritic calcite is always associated with both slightly higher $\delta^{18}O$ values (compared to the brown laminated calcite) and positive $\delta^{13}C$ excursions (light

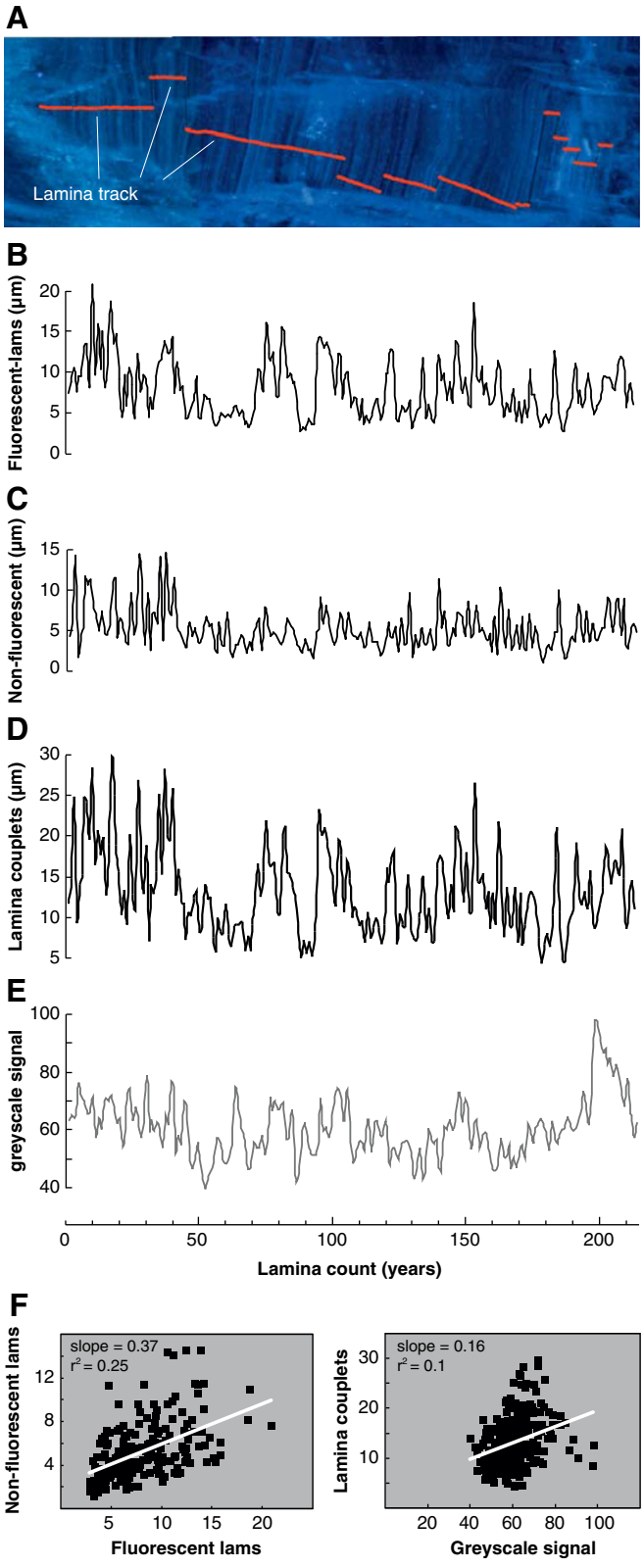

Fig. 6. Lamination analysis (lamina track 1) of brown laminated calcite in core TKS I. Top: Epifluorescence photomicrographs merged into a seamless image and displaying a continuous sequence of UV-laminae and the lamina track along which the lamina analysis was performed. The thickness records for the fluorescent calcite bands, the non-fluorescent calcite bands and the lamina couplets (i.e. fluorescent plus non-fluorescent calcite bands) are shown together with the greyscale curve. Bottom: Cross plots between fluorescent and non-fluorescent calcite bands showing notable correlation. Cross plot between the lamina couplets and the greyscale curve shows no significant correlation.

grey bars in Fig. 7A and B). C isotope data of the brown laminated calcite packages in particular show a high-amplitude, high-frequency signal. The irregular high-amplitude $\delta^{18}O$ signal measured near the top of all TKS cores (i.e. from 0 to ~4 mm) coincides with the topmost macroscopically thin, laminated calcite unit (dark grey bars in Fig. 7A and B).

5.6. Energy-dispersive XRF analysis

The elemental concentration of those elements that were above the detection limit and revealed significant changes between the brown detrital-rich calcite and white inclusion-poor calcite is displayed in Table 2. All calcite fabrics reveal low Mg, Sr and Ba concentrations (<2250 ppm), but Al, Si and Fe are much more abundant in the brown laminated and brown dendritic calcite as compared to the white-inclusion poor calcite (by one to three orders of magnitude).

6. U–Th dating

Seven U–Th samples were taken from the cores TKS I and IV and referenced to core TKS I (Fig. 4, Table 3). All U–Th samples are variably compromised by detrital Th. Samples from the top 8 mm of the TKS cores were discarded because the correction yielded unacceptably large age uncertainties. Significant detrital Th was encountered in sample 3718 (from the dendritic calcite just above hiatus H2) and 3717 (from the brown laminated calcite package at 62 mm depth), while relatively clean samples were obtained from the white translucent calcite layer that is intercalated into the brown laminated calcite package at 68 mm depth (i.e. samples 3804 and 3823; Table 3).

7. Discussion

7.1. Detrital content

^{232}Th concentration in the white calcite layer within the brown laminated calcite sequence is low (i.e. 2.59 ± 0.04 ng/g — sample 3804, 6.29 ± 0.04 ng/g — sample 3823; Table 3) and is comparable to ^{232}Th concentrations in the white inclusion-poor MIS 5e and 5d calcite (2.62 ± 3.30 ng/g on average; Meyer et al., 2008). In all other samples obtained from the brown calcite succession ^{232}Th concentrations is higher by an order of magnitude (Table 3). Th is known to strongly adsorb to particles and colloids, chiefly clay minerals and Fe-oxyhydroxides derived from the weathering zone (i.e. Lead and Wilkinson, 2006; Degueldre and Kline, 2007). This is supported by the EDS-XRF analysis indicating much higher Al, Si and Fe concentrations in the brown laminated and dendritic calcite packages compared to the white inclusion-poor calcite deposited during MIS 5e (Table 2).

7.2. Calcite fabric

The type of calcite fabric is mainly governed by the interplay of three parameters: supersaturation, outgassing, and discharge (Dreybrodt, 1988; Gonzalez et al., 1992) and at least for alpine flowstones (modern and ancient) discharge seems to be the most important controlling parameter (Frisia et al., 2000). Frisia et al. (2000) showed that a dendritic fabric results from calcite precipitation during periods of highly variable but mostly very low drip rate. During dry periods prolonged outgassing occurs which in turn gives rise to a high degree of supersaturation and isotopic disequilibrium. The columnar calcite fabric (as observed in the brown laminated calcite packages) forms when speleothems are continuously wet (i.e. under stable hydrological karst conditions and at constant flow of seepage water), and from fluids at low degrees of supersaturation (Gonzalez et al., 1992; Frisia et al., 2000). Macroscopic petrography also suggests that the entire TKS flowstone surface was covered by a more or less continuous water film during columnar calcite growth, because individual macroscopic laminae can be traced between

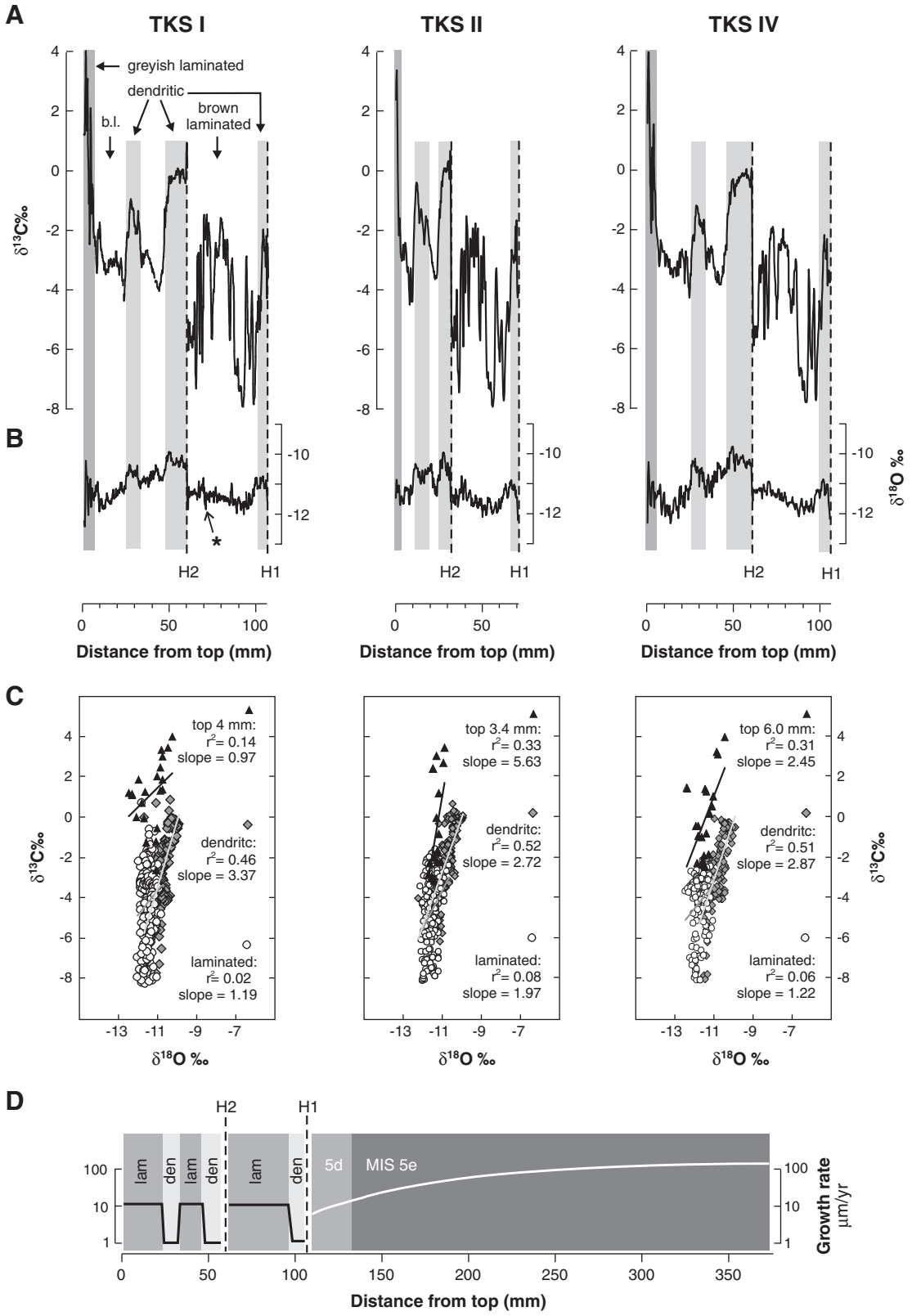

Fig. 7. Stable isotope record of the brown, detrital-rich calcite of cores TKS I, II and IV. A and B: Carbon and oxygen isotope profiles. An arrow and an asterisk mark the position of the white translucent calcite layer which is intercalated into the brown laminated calcite sequence. The most precise U–Th ages were derived from this layer (samples 3804 and 3823; Table 1). C: Isotope cross plots. D: Growth rates for the white inclusion-poor MIS 5e and 5d calcite (based on 20 U–Th ages; Meyer et al., 2008) and for the brown detrital-rich calcite sequence (inferred from fabric and UV-lamination observations, see text).

the cores (Fig. 3). Nevertheless, the thickness of individual calcite layers is not constant in the cores indicating that flowstone growth rates were spatially and temporally variable (Fig. 4).

Close examination of the brown calcite sequence further revealed a complex succession of dendritic and laminated calcite and the presence of dendritic micro-layers (Fig. 4). We therefore conclude

Table 2
U–Th ages of the brown, detrital-rich calcite of the TKS flowstone (n.a. = not available).

Sample	Depth	dU (corr.)	Error	^{238}U	Error	^{232}Th	Error	^{230}Th	Error	Age uncorrected	Age corrected	Error (2 sigma)	
	(cm)	(‰)	(abso.)	(μg/g)	(abso.)	(ng/g)	(abso.)	(pg/g)	(abso.)	(ka)	(ka)	+ (ka)	− (ka)
3719	0	242.8	6.7	0.06098	0.00012	76.84	0.32	0.6155	0.0092	n.a.	n.a.	n.a.	n.a.
3853	0.83	315.7	22.7	0.08594	0.00025	155.04	3.41	0.9193	0.0616	n.a.	n.a.	n.a.	n.a.
3854	0.8	262.4	10.7	0.08709	0.00017	133.80	0.86	0.930	0.022	n.a.	n.a.	n.a.	n.a.
3718	5.1	140.8	9.6	0.08606	0.00017	43.25	0.40	0.836	0.019	80.7	67.4	22.0	15.7
3717	6.2	161.3	3.6	0.06580	0.00013	20.418	0.078	0.689	0.011	86.9	79.1	13.7	11.0
3804	6.8	142.0	7.2	0.05640	0.00011	2.594	0.039	0.603	0.021	90.7	89.6	5.4	5.4
3823	7.1	143.2	5.8	0.08680	0.00017	6.296	0.042	0.914	0.020	88.7	86.9	4.4	4.4

that the cave hydrology apparently fluctuated between dry episodes with very low drip rates (formation of dendritic calcite packages and dendritic micro-layers) and more humid periods with constant seepage flow (columnar calcite growth).

7.3. Speleothem fluorescence and lamina analysis

Fluorescence in speleothems is – in most instances – caused by organic molecules (mainly humic and fulvic acids), which are derived from the overlying soil and were transported with the karst water onto the speleothem (Shopov et al., 1994; Baker et al., 1996; Tan et al., 2006; Baker et al., 2008). In alpine catchments a seasonal peak of dissolved organic carbon concentration in rivers (and hence groundwater) occurs in spring, due to snowmelt (Boyer et al., 1997), and this process has been invoked to account for annual luminescent banding in arctic and alpine speleothems (Linge et al., 2001, 2009; Baker et al., 2008).

In some cases fluorescence in cave calcites can be attributed to the presence of aragonite or microbes (living in-situ on the speleothem) rather than to flushing of organic substances from the infiltration area (Ortega et al., 2005; Jones, 2010). However, we have no petrographical or geochemical indication to suggest that fluorescence in the TKS flowstone (neither in the brown-laminated calcite, nor in the dendritic calcite nor in the white inclusion-poor MIS 5e and d calcite) is caused by aragonite (i.e. no aragonitic fabrics or relict textures; low Sr and U concentrations; Frisia, 1996; McMillan et al., 2005; Ortega et al., 2005) or by microbial activity (no fabrics, structures or isotopic signatures consistent with microbial activity; Gradzinsky, 2001; 2003; Jones, 2010). Indeed, the regular succession of fluorescent and non-fluorescent laminae in the brown laminated calcite sequence of the TKS cores (Figs. 5C and 6A) rather suggests organic fluxes possibly controlled by intra-annual or multi-annual climate variability. Considering EKC's high-alpine infiltration area it is reasonable to propose that fluorescent calcite precipitated in response to seasonal snowmelt (while non-fluorescent calcite formed during the rest of the year), which in turn would imply annual cyclicity and the presence of soil and some sort of vegetation cover above the cave.

Continuous sequences with fluorescence micro-banding exist in the TKS flowstone with individual lamina couplets between 5 and 30 μm in thickness (average 11 ± 5 μm; Fig. 6). If these couplets are indeed annual in origin, the thickness record can be used to estimate growth rates for selected flowstone sequences. Such growth rate estimates are at the lower end of the range of measured growth rates of modern flowstones (Baker and Smart, 1995). Slow flowstone accretion might have been maintained for many decades and up to ca. two centuries in the case of the lamina track 1 (i.e. continuous lamination lacking corrosion or hiati; Fig. 6).

Dendritic calcite is devoid of micro-banding under epifluorescence, yet displays diffuse and sometimes strong fluorescence (Fig. 5B and D). As discussed above, we invoke organic molecules but exclude aragonite or microbial activity as causes for the observed fluorescence. The most likely explanation for the fluorescence properties of the dendritic calcite and the simultaneous absence of fluorescence banding is that the very low drip rates in combination with the occasional high discharge events prevented seasonal karst water pulses to reach the flowstone surface but rather facilitated mixing of seasonal surface signals en route through the thick karst aquifer.

7.4. Corrosion horizons

In the brown detrital-rich calcite sequence of the TKS core corrosion horizons can be frequently observed under the epifluorescence microscope. They appear as faint, irregular boundaries that cut into pre-existing laminae or into the dendritic crystal fabric (Fig. 5B, D and E). We believe that no major stillstand in flowstone deposition was associated with the majority of these corrosion horizons, because detritus or inclusion-rich layers are usually lacking. Some corrosion features are laterally discontinuous or dissolved only a small fraction of the former flowstone surface. Most of the corrosion horizons are therefore best described as micro-hiati that are probably associated with time gaps of less than a few years. They might represent extreme hydrological events or periods during which enhanced discharge through both, the soil zone and the karst aquifer resulted in a drop of the degree of supersaturation of the seepage water and hence dissolution of the flowstone surface. Corrosion by condensation might be invoked as well to explain these dissolution features, however, corrosion residues or micritisation of the speleothem calcite as typical for condensation corrosion (Martin-Garcia et al., 2011) are generally lacking and we therefore suggest that corrosion by condensation was only of minor importance.

Intensive corrosion is associated with the major hiati H1 and H2 (Fig. 5A and B). Also, the calcite fabric changes suddenly and isotopic jumps occur at these boundaries and detrital and organic-rich layers formed on top of both hiati, suggesting that H1 and H2 demarcate major growth cessations. Between the hiati H1 and H2 we mapped the corrosion horizons in detail and found no correlation with the isotope record, supporting the interpretation that many of these corrosion features represent micro-hiati rather than significant gaps or halts in flowstone deposition (Fig. 8).

Table 3
Energy-dispersive X-ray fluorescence analysis for selected macroscopic calcite fabrics (b.d.l. — below detection limit).

Calcite type	Mg (ppm)	Sr (ppm)	Ba (ppm)	Al (ppm)	Si (ppm)	Fe (ppm)	Th (ppm)	U (ppm)
Brown dendritic	2226	56	b.d.l.	813	2271	382	2	b.d.l.
Brown laminated	1098	43	15	957	2894	315	4	b.d.l.
White inclusion-poor	922	64	b.d.l.	6	799	b.d.l.	b.d.l.	b.d.l.

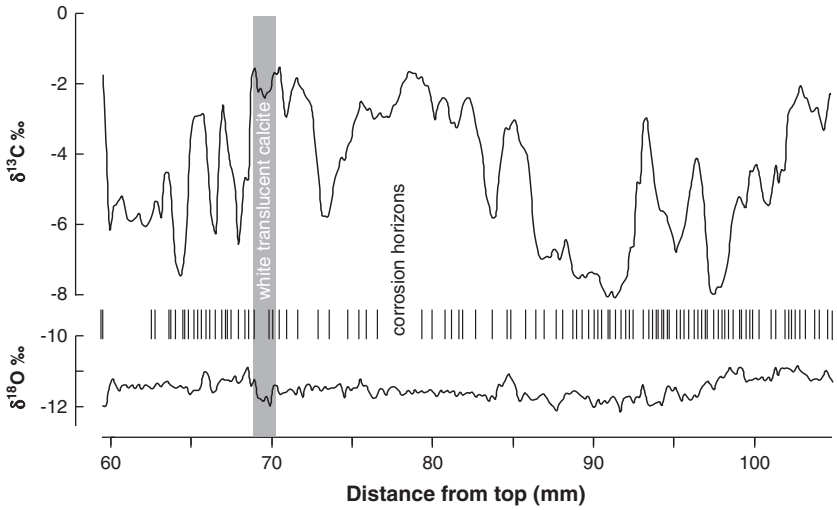

Fig. 8. Stable isotope record of the TKS I core and position of the corrosion horizons between the hiati H1 and H2. A total of 111 corrosion horizons were identified. Note lack of a correlation between corrosion features and isotope data.

Near the top of the TKS flowstone (i.e. above ~4.5 mm depth) white laminae alternate with brownish to greyish detrital-rich laminae that are associated with an irregular high-amplitude high-frequency isotope signal and frequent corrosion horizons (Figs. 5E and 7). Major growth cessations might be linked with these corrosion events, but we are unable to resolve this extremely thinly laminated top part of the TKS flowstone.

7.5. Stable isotopes and isotopic equilibrium vs. disequilibrium

Flowstones are well known for their potentially complex growth morphology resulting in a laterally discontinuous internal stratigraphy, in particular if multiple sources of drip or splash water are present and if the speleothem is laterally extensive. In the case of the TKS flowstone, however, the conical shape and a single feeding fracture suggest that seepage was sourced from a single point. Importantly, the isotope record of all three TKS cores reveals a remarkable degree of consistency (despite the fact that the cores come from positions between ~50 cm and more than 100 cm apart from each other; Figs. 3 and 7). Because the same isotopic features and first-order trends can be seen in all cores we argue that they reflect climatic trends rather than features specific to different locations on the surface of the TKS flowstone and thus internal growth dynamics during speleothem formation.

Prior to identifying paleoenvironmental or climatic proxy information from the stable isotope data it is essential to evaluate the degree of equilibrium conditions during speleothem growth (e.g., Mickler et al., 2004, 2006). As a modern proxy calibration for $\delta^{18}O$ and 'Hendy tests' (Hendy, 1971) is not feasible in the case of the ancient TKS flowstone, we follow an alternative approach: equilibrium versus kinetic fractionation during calcite precipitation is evaluated by analysing the correlation between the $\delta^{13}C$ and $\delta^{18}O$ values which were sampled continuously along each core (cf. Mickler et al., 2004, 2006; Wiedner et al., 2008). This was done for each core and each calcite fabric separately, i.e. for the dendritic calcite and for the brown laminated calcite (columnar fabric), as well as for the topmost part of each core (displaying the irregular high-amplitude, high-frequency signal; Fig. 7C).

The results suggest that the isotopic composition of the different calcite fabrics reflects non-equilibrium isotope effects (i.e. by kinetic fractionation due to rapid CO_2-degassing and evaporation) to different degrees.

Kinetic fractionation due to CO_2-degassing results in enrichment in ^{13}C in the precipitated carbonate, while the oxygen isotopic composition is generally less affected by kinetic enrichment because of the buffering effect of the water reservoir (Mickler et al., 2004; Romanov et al., 2008; Mühlinghaus et al., 2009). Experimental evidence (Mickler et al., 2006; Wiedner et al., 2008; Mühlinghaus et al., 2009) shows that if degassing is fast the $\delta^{18}O$ and $\delta^{13}C$ values co-vary ($\Delta^{13}C/\Delta^{18}O$ slope of 1.4 ± 0.6). In the case of slow degassing the oxygen isotope composition is buffered which results in virtually no change of the $\delta^{18}O$ value of the precipitate and hence a slope that approaches an infinite value. Evaporation also causes kinetic enrichment in the precipitated carbonate (Hendy, 1971; Mickler et al., 2006).

For flowstones it has been demonstrated that the thickness of the water-film has a first-order control on kinetic fractionation; i.e. low discharge promotes a thin water-film which in turn favours CO_2 degassing and evaporation, hence kinetic isotope enrichment (Boch and Spötl, 2011). Cave ventilation can also enhance degassing (and thus kinetic fractionation; e.g. Spötl et al., 2005), however, this process is considered insignificant for the interior part of EKC from where the TKS samples were retrieved.

The isotope cross plots in Fig. 7C suggest that for the dendritic calcite fabric slow degassing (from a very thin water film) controlled the $\delta^{13}C$ values (steep $\Delta^{13}C/\Delta^{18}O$ slopes of 2.72–3.37; r^2: 0.3–0.5), which is in-line with the suggestion of Frisia et al. (2000) of dendritic calcite formation under a very low discharge regime. The brown laminated calcite (composed of columnar calcite fabric) reveals a $\Delta^{13}C/\Delta^{18}O$ slope between 1.22 and 1.97, indicative of faster degassing and less effective oxygen isotope buffering. Kinetic enrichment might occur under low rates of flowstone accretion (i.e. ~11 μm/yr; assuming an annual origin of the UV-fluorescent lamina couplets and using the average lamina thickness, see above). We further observe systematically higher $\delta^{18}O$ values in the dendritic calcite compared to the laminated calcite fabrics. We argue that the extremely dry climatic conditions during these time intervals (as indicated by the dendritic fabric) probably resulted in slight evaporation and thus slightly higher $\delta^{18}O$ values compared to those of the brown laminated calcite (Frisia et al., 2000; Mickler et al., 2006). Finally, it appears that slow CO_2 degassing was most pronounced near the top of the TKS flowstone, where the highest $\delta^{13}C$ values are encountered (while $\delta^{18}O$ values remain similar to that of the brown laminated calcite).

7.6. Timing of calcite deposition

The most reliable ages are from samples 3804 and 3823 (the white translucent calcite layer at 68 mm depth in core TKS I; at 72 mm depth in core TKS IV; Fig. 4). Detrital Th contamination is significantly less in these samples and the corrected ages suggest calcite deposition at 88.3 ± 6.9 ka (averaged age, 2σ errors combined in quadrature;

Table 3). Comparison of these ages with the NGRIP $\delta^{18}O$ record suggests white inclusion-poor calcite precipitation during Greenland Interstadial (GIS) 21 or 22 or during the respective Greenland stadials (GS; Fig. 9). An average lamina thickness of ~11 ± 5 μm was deduced via lamination analysis for the brown laminated calcite package between 96 and 59 mm depth (core TKS I) that also encompasses the U–Th dated white translucent calcite layer (Fig. 4). Assuming an annual origin for these fluorescent calcite couplets we roughly estimate a growth duration of ~3600 ± 1650 yr for this brown laminated calcite package. No major growth cessations are present in this part of the TKS core (although micro-hiati are common) and we therefore interpret the brown laminated calcite sequence as an expression of almost continuous calcite precipitation during the early part of the last glacial cycle (i.e. MIS 5a and/or 5b).

The timing of brown dendritic calcite precipitation is difficult to constrain. Samples 3717 and 3718 (directly obtained from the dendritic calcite above hiatus H2; Table 3) yielded ages of 79 and 67 ka, respectively. The very large errors, however, preclude a correlation of this dendritic calcite package with individual GS or GIS (Fig. 9).

The three U–Th samples obtained from the thinly laminated top part of the TKS flowstone (i.e. between 0 and 4 mm; samples 3719, 3853, 3854; Table 3) were discarded because of their very high detrital ^{232}Th content. Nevertheless, we know from ^{14}C-dated clastic cave sediments in EKC that back-flooding of the cave occurred during the LGM (see above and Table 1), which gave rise to the deposition of greyish silt and clay in the upper cave level. This greyish cover also coats the TKS flowstone, thus providing a minimum age for the top-most calcite in the TKS cores (i.e. the thinly laminated whitish and greyish calcite between 0 and 4 mm must be older than MIS 2). It is therefore possible that the complex succession of brown detrital-rich dendritic as well as laminated calcite above hiatus H2 was deposited in repeated pulses during the middle part of the last glacial cycle (i.e. MIS 3 and/or 4).

8. Paleoenvironmental interpretation

The growth cessation at ca. 114 ka (i.e. hiatus H1) in the TKS flowstone demarcates the onset of MIS 5d interstadial conditions in the alpine realm (Meyer et al., 2008) and can be correlated with the cold event C24 which has been identified throughout the North Atlantic and which had a major impact on the climate of Europe (e.g. Chapman and Shackleton, 1999; McManus et al., 2002; Shackleton et al., 2002; Müller and Kukla, 2004; Drysdale et al., 2007). The high detrital content and the different calcite fabrics above hiatus H1 compared to the white, inclusion-poor MIS 5e and 5d calcite below H1 suggest that at least some of the environmental parameters changed fundamentally (and durably) after 114 ka for EKC.

A possible explanation to account for the sudden petrographic and isotopic changes above hiatus H1 involves rates of detrital fluxes during flowstone growth. If the flux of detrital material from the infiltration area into EKC was constant over time but rates of calcite deposition decreased rapidly in response climatic deterioration, brown detrital-rich calcite might have precipitated. This simple model is unlikely, however, considering that the expected growth rates for the brown detrital-rich calcite are on the same order of magnitude as the growth rates that have been determined for the MIS 5d calcite, i.e. the white and inclusion-poor calcite that precipitated immediately prior to 114 ka (Fig. 7D). We also reject back-flooding of the cave as a possible explanation because the brown calcite is contaminated by particles that seeped through the karst aquifer (high ^{230}Th, Si, Al and Fe concentrations) but lacks clastic layers that would suggest flooding.

Important for this paleoenvironmental discussion is the geomorphological setting of EKC. The infiltration area of EKC is in a high-alpine position (mean elevation ~1900 m) and composed of steep ridges and basins. Despite a thickness of almost 1000 m of the vadose zone above the cave (entrance at 1040 m), a good hydrological connectivity between the infiltration area and EKC was demonstrated by tracer experiments (Ganahl, 1991). Routing of karst water through the vadose zone is further facilitated by tectonic structures (i.e. ENE trending axial-plane foliation and strike-slip faults) that are pervasive and steeply dipping in this region (Exner, 1979; Peer and Zimmer, 1980; Wang and Neubauer, 1998).

8.1. Geomorphological processes in a high-alpine catchment

In alpine catchments glacial and periglacial processes (e.g., glacial erosion, permafrost creep and solifluction) in conjunction with the vegetation cover are key factors in controlling weathering and erosion rates and thus the abundance of sediment in discharging waters (Gurnell, 1987; Patzelt, 1994; Höfner, 1995; Hinderer, 1999, 2001; van

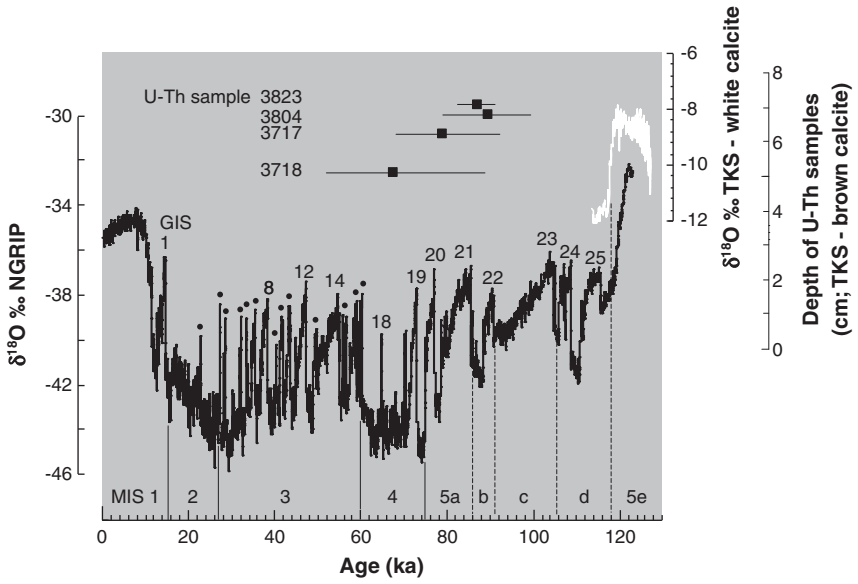

Fig. 9. TKS flowstone in the climatic context of the last glacial/interglacial cycle. The U–Th ages (2 sigma errors) from the brown detrital-rich calcite sequence are plotted in conjunction with the $\delta^{18}O$ record from NGRIP (black curve; North Greenland Ice Core Project members, 2004) and the $\delta^{18}O$ record from the white, inclusion-free calcite sequence of the TKS flowstone (white curve; Meyer et al., 2008). Greenland Interstadials (GIS) are flagged (either with their respective number or as black dots).

Husen, 2000; Ballantyne, 2002; Schulte et al., 2008). While glacial erosion and permafrost creep dominate high-alpine peaks and catchments (i.e. >2500 m asl in the Central Alps today), solifluction above non-permanently frozen ground is important also in catchments of intermediate altitudes (2500–2300 m asl; Veit, 2002). Solifluction is caused by annual and diurnal freezing and thawing of the subsurface which results in frost weathering but also in downslope creeping of the water-saturated top soil and hence erosion (Hales and Roering, 2005, 2007; Matsuoka, 2005). Substantial amounts of fine-grained sediment are produced and transported by this mechanism (Höfner, 1995; Jaesche, 1999) and further chemical weathering increases the suspended sediment concentration in the water entering the karst aquifer. Vegetation, at the other hand, stabilises sediment, e.g. on steep slopes. Both processes (i.e. the stabilizing effect of vegetation on sediment-mantled slopes and solifluction) are sensitive to temperature changes (Haeberli, 1983; Veit, 2002). Prolonged cooling intensifies solifluction and reduces vegetation (and ultimately initiate glacier formation), while sustained warming results in a vegetated and thus geomorphologically stable catchment with little or no availability of detrital material (as today).

In the central Eastern Alps the lower limit of (discontinuous) mountain permafrost coincides with the −2 °C isotherm and lies at ca. ~2500 m today (Barsch, 1978; Haeberli, 1983; Kerschner, 1985; Lieb, 1998), while active solifluction occurs down to an altitude of ~2300 m asl in the same area (Veit, 2002). It is evident that a moderate depression of these periglacial limits by a few hundred metres will affect the infiltration area of the EKC already. Cool climatic conditions generally prevailed subsequent to 114 ka, entailing at least an episodical enhancement of periglacial and glacial activity in high-alpine catchments, which in turn would have allowed sediment-laden melt water and fine-grained sediment to enter the karst aquifer. While coarser material (i.e. ≥ silt fraction) was probably filtered out in the vadose zone, the colloids seeped through and ultimately became trapped in the flowstone during calcite precipitation, as also suggested by the high concentrations of ^{232}Th (Table 3) as well as Al, Si and Fe (Table 2).

8.2. Speleothem precipitation at the glaciation threshold — a depositional model for EKC and temperature estimates

As outlined above, we regard the impact of cold climatic conditions on the high-alpine infiltration area of EKC as the most plausible mechanism to explain the formation of the brown detrital-rich calcite sequence. For the brown laminated calcite packages (columnar calcite fabric and fluorescent lamination) petrographic and isotopic data further suggest the presence of some vegetation in the infiltration area and calcite precipitation from a thin but continuous water film. These observations suggest a cool and dry climate which still allowed speleothem growth. During dendritic calcite formation enhanced kinetic fractionation suggest even drier conditions and we speculate that this calcite fabric might have been precipitated during stadials, when the infiltration area of EKC was close to the glaciation threshold (sensu Porter, 1977; i.e. no glaciers in the infiltration area) but the mean annual air temperature (MAAT) in EKC still above the freezing point (i.e. no cave freezing).

A simple calculation allows constraining the maximum temperature depression that is conceivable before cave freezing occurs and speleothem deposition ceases. Liquid water is required for speleothem formation implying that the interior cave temperature stayed above 0 °C during precipitating brown detrital-rich calcite. The interior cave temperature closely tracks the MAAT outside a cave (Wigley and Brown, 1976). Today the temperature in EKC is 5.5 °C, while the 0 °C isotherm lies at 2200 m. Using an environmental lapse rate of 0.5 °C/100 m (based on 17 high and low alpine meteorological stations in the vicinity of EKC) and the altitude difference between EKC and the 0 °C isotherm (i.e. 1160 m) the MAAT could have decreased by a maximum of ~5.8 °C. Hence, a sustained temperature depression of >6 °C is likely to have caused freezing in EKC, which in turn would likely be recorded as a major hiatus in the flowstone (e.g. hiati H1 or H2).

In a similar way a rough estimate of the amount of cooling that is required to initiate periglacial activity in the infiltration area of EKC and thus start precipitation of brown detrital-rich calcite can be made. The 2500 m contour demarcates the lower limit of (discontinuous) permafrost in the Alps. This periglacial limit coincides with the −2 °C isotherm (see above) and is known to be temperature-dependent but insensitive to precipitation changes (Barsch, 1978; Haeberli, 1983). Between 2300 and 2500 m solifluction over non-permanently frozen ground occurs in the central Eastern Alps today (Barsch, 1978; Kerschner, 1985; Lieb, 1998; Veit, 2002) and lowering this altitudinal solifluction range by ~500 m causes a complete overlap with the present-day infiltration area of EKC. Using the lapse rate from above a value of ~2.5 °C can be calculated as a ballpark figure for the minimum temperature depression required for initiating solifluction above EKC and hence brown detrital-rich calcite precipitation on the TKS flowstone.

Petrographic investigations and isotopic modelling (Meyer et al., 2008) for the white, inclusion-poor calcite of the TKS core formed during the MIS 5e and the beginning of the MIS 5d indicate that during interglacial conditions and the MIS 5e/d transition stable geomorphological conditions prevailed in the infiltration area of EKC. White calcite also occurs in the brown (glacial) part of the TKS flowstone as individual (up to 4 mm thin) calcite layers and we therefore propose that brown laminated calcite precipitation might have been punctuated by milder, geomorphologically stable episodes (i.e. long interstadials with reduced solifluction and frost shattering and some vegetation that stabilized the slopes above EKC).

9. Conclusions

The studied flowstone consists of a lower white, inclusion-poor calcite unit that precipitated between ca 127 and 114 ka (Meyer et al., 2008) and an upper brown, detrital-rich calcite sequence that formed intermittently during subsequent stadials and interstadials. This study elaborates on this brown, detrital-rich flowstone succession and suggests that the petrographic and isotopic data are best interpreted as the result of millennial-scale climate fluctuations that impacted on the high-alpine catchment area of EKC. Permafrost, periglacial processes and vegetation in high-alpine catchments are highly sensitive to temperature changes, hence are believed to have determined the amount of sediment-laden water infiltrating into the karst aquifer and thus the detritus content as well as the calcite fabric of the TKS flowstone. According to our estimates a few degrees of cooling (~2.5 °C) were required to initiate solifluction above EKC, while cave freezing occurred as the MAAT plunged by more than 6 °C. We propose that within this temperature range a depositional continuum exists for EKC: brown laminated calcite (displaying a columnar fabric) precipitated once the periglacial activity became intensive enough in the infiltration area (≥2.5 °C cooling) while further drying (and possibly also cooling) resulted in a dendritic fabric. Major growth cessations (e.g. hiati H1 and H2) are interpreted as the result of cave freezing (>6 °C cooling). White inclusion-poor calcite precipitated during warm and geomorphologically stable periods in EKC (i.e. under conditions roughly similar to today or the last interglacial; Meyer et al., 2008). White calcite layers intercalated with the brown detrital-rich calcite sequence might therefore reflect warm and geomorphologically stable interstadials. Reliable U–Th ages from one of these white inclusion-poor calcite bands indicate calcite deposition during GIS 21 or 22 (i.e. MIS 5a or b). The high detrital content in most other calcite packages precludes precise U–Th ages to be determined. U–Th isochron dating would be a valuable next step to further constrain the timing of these episodes of speleothem deposition during the early and middle parts of the last glacial cycle when the catchment was most of the time close to the glaciation threshold.

Acknowledgments

We thank the federal government of Salzburg for sampling permission in the Entrische Kirche and R. Erlmoser for kind assistance in the cave. The basemap for Fig. 1 was kindly provided by R. Starnberger. This research was funded by the Austrian Science Fund (FWF, grant Y122-GEO to CS). MCM was funded by the 7th Framework Programme of the EU (grant IOF-GEOPAL-219944) during the writing stage. We thank the reviewers as well as G. Zanchetta and J. Reitner for their helpful comments on an earlier version of the manuscript.

References

Ayalon, A., Bar-Matthews, M., Kaufman, A., 1999. Petrography, strontium, barium and uranium concentrations, and strontium and uranium isotope ratios in speleothems as palaeoclimatic proxies: Soreq Cave, Israel. The Holocene 9, 715–722.
Baker, A., Smart, P.L., 1995. Recent flowstone growth rates: field measurements in comparison to theoretical predictions. Chemical Geology 122, 121.
Baker, A., Barnes, W.L., Smart, P.L., 1996. Speleothem luminescence intensity and spectral characteristics: signal calibration and a record of palaeovegetation change. Chemical Geology 130, 65–76.
Baker, A., Smith, C.L., Jex, C., Fairchild, I.J., Genty, D., Fuller, L., 2008. Annually laminated speleothems: a review. International Journal of Speleology 37, 193–206.
Ballantyne, C.K., 2002. Paraglacial geomorphology. Quaternary Science Review 21, 1935–2017.
Barsch, D., 1978. Rock glaciers as indicators for discontinuous alpine permafrost: an example from the Swiss Alps. : Proceedings of the Third International Conference on Permafrost, v. 1. National Research Council of Canada, Edmonton, pp. 349–352. July 10–13.
Boch, R., Spötl, C., 2011. Reconstructing paleoprecipitation from an active cave flowstone. Journal of Quaternary Sciences 26, 675–687.
Boch, R., Cheng, H., Spötl, C., Edwards, R.L., Wang, X., Häuselmann, P., 2011. NALPS: a precisely dated European climate record 120–60 ka. Climate of the Past 7, 1049–1072.
Boyer, E.W., Hornberger, G.M., Bencala, K.E., McKnight, D.M., 1997. Response characteristics of DOC flushing in an alpine catchment. Hydrological Processes 11, 1635–1647.
Chapman, M.R., Shackleton, N.J., 1999. Global ice-volume fluctuations, North Atlantic ice-rafted events, and deep-ocean circulation changes between 130 and 70 ka. Geology 27, 795–798.
Cheng, H., Edwards, R.L., Hoff, J., Gallup, C.D., Richards, D.A., Asmerom, Y., 2000. The half-lives of uranium-234 and thorium-230. Chemical Geology 169, 17–33.
Degueldre, C., Kline, A., 2007. Study of thorium association and surface precipitation on colloids. Earth and Planetary Science Letters 264, 104–113.
Dreybrodt, W., 1988. Processes in Karst Systems. Springer, Berlin.
Drysdale, R.N., Zanchetta, G., Hellstrom, J.C., Fallick, A.E., McDonald, J., Cartwright, I., 2007. Stalagmite evidence for the precise timing of N Atlantic cold events during the early last glacial. Geology 25, 77–80.
Ehlers, J., Gibbard, P.L., 2004. Quaternary glaciations — extent and chronology. Part I: Europe. : Developments in Quaternary Sciences, 2. Elsevier.
Exner, C., 1979. Geolgie des Salzachtales zwischen Taxenbach und Lend. Jahrbuch der Geologischen Bundesanstalt 122, 1–73.
Fairchild, Ian J., Treble, Pauline C., 2009. Trace elements in speleothems as recorders of environmental change. Quaternary Science Reviews 28, 449–468.
Forbes, M.S., Bestland, E.A., 2007. Origin of the sedimentary deposits of the Naracoorte Caves, South Australia. Geomorphology 86, 369–392.
Frisia, S., 1996. Petrographic evidences of diagenesis in speleothems: some examples. Speleochronos 7, 21–30.
Frisia, S., Borsato, A., Fairchild, I.J., McDermott, F., 2000. Calcite fabrics, growth mechanisms and environments of formation in speleothems from the Italian Alps and southwestern Ireland. Journal of Sedimentary Research 70, 1183–1196.
Frumkin, A., Stein, M., 2004. The Sahara–East Mediterranean dust and climate connection revealed by strontium and uranium isotopes in a Jerusalem speleothem. Earth and Planetary Science Letters 217, 451–464.
Ganahl, P., 1991. Ersatzwasserversrogung für Schwarzach infolge der Staustufe Wallnerau: Österr. Zeitschrift Energiewirtschaft 44, 86–92.
Goede, A., McCulloch, M., McDermott, F., Hawkesworth, C., 1998. Aeolian contribution to strontium and strontium isotope variations in a Tasmanian speleothem. Chemical Geology 149, 37–50.
Gonzalez, L.A., Carpenter, S.J., Lohmann, K.C., 1992. Inorganic calcite morphology: roles of fluid chemistry and fluid flow. Journal of Sedimentary Petrology 62, 382–399.
Gradzinsky, M., 2001. Role of bacteria in the growth of cave pearls. 13th International Congress of Speleology, pp. 205–281.
Gradzinsky, M., 2003. Bacterial influence on speleothem oxygen isotope composition: an example based on cave pisoids from Perlova cave (Slovakia). Geologica Carpathica 54, 199–204.
Gurnell, A.M., 1987. Fluvial sediment yield from alpine, glacierized catchments. In: Clark, M.J., Gurnell, A.M. (Eds.), Glacio-fluvial Sediment Transfer. John Wiley, pp. 415–420.
Haeberli, W., 1983. Permafrost–glacier relationships in the Swiss Alps today and in the past. Proceedings of the Permafrost: Fourth International Conference on Permafrost, Fairbanks, Alaska, pp. 415–420.
Hales, T.C., Roering, J.J., 2005. Climate-controlled variations in scree production, Southern Alps, New Zealand. Geology 33, 701–704.
Hales, T.C., Roering, J.J., 2007. Climatic controls on frost cracking and implications for the evolution of bedrock landscapes. Journal of Geophysical Research, Earth Surface 112, F02033.
Henderson, G.M., 2006. Caving into new chronologies. Science 313, 620–622.
Hendy, C.H., 1971. The isotopic geochemistry of speleothems. 1. The calculation of the effects of the different modes of formation on the isotopic composition of speleothems and their applicability as palaeoclimatic indicators. Geochimica et Cosmochimica Acta 35, 801–824.
Hinderer, M., 1999. Klimagesteuerte Denduations-Sedimentakkumulations-Systeme: Massenbilanz, Modellierung und Anwendung. Geowissenschaftliche Fakultät der Universität Tübingen. Unpubl. Habilitation.
Hinderer, M., 2001. Late Quaternary denudation of the Alps, valley and lake fillings and modern river loads. Geodinamica Acta 14, 231–263.
Hoffmann, D.L., Prytulak, J., Richards, D.A., Elliott, T., Coath, C.D., Smart, P.L., Scholz, D., 2007. Procedures for accurate U and Th isotope measurements by high precision MC-ICPMS. International Journal of Mass Spectrometry 264, 97–109.
Höfner, T., 1995. Fluvial dynamics in the periglacial belt of the Central Austrian Alps. Zeitschrift für Geomorphologie N.F. Supplementbände 100, 159–166.
Holzkämper, S., Spötl, C., Mangini, A., 2005. High-precision constraints on timing of Alpine warm periods during the middle to late Pleistocene using speleothem growth periods. Earth and Planetary Science Letters 236, 751–764.
Hu, C., Huang, J., Fang, N., Xie, S., Henderson, G.M., Cai, Y., 2005. Adsorbed silica in stalagmite carbonate and its relationship to past rainfall. Geochimica et Cosmochimica Acta 69, 2285–2292.
Ivy-Ochs, S., Kerschner, H., Reuther, A., Preusser, F., Heine, K., Maisch, M., Kubik, W.P., Schlüchter, C., 2008. Chronology of the last glacial cycle in the European Alps. Journal of Quaternary Science 23, 559–573.
Jaesche, P., 1999. Bodenfrost und Solifluktionsdynamik in einem alpinen Periglazialgebiet (Hohe Tauern, Osstirol). Bayreuther Geowissenschaftliche Arbeiten 20, 1–136.
Jaillet, S., Pons-Branchu, E., Maire, R., Hamelin, B., Brulhet, J., 2006. Record of Holocene palaeo-groundwater floods in two stalagmites of the Rupt-Du-Puits Sytem (Barrois, France). Morphological analysis of laminae and U/Th tims datings. Geologica Belgica 9, 297–307.
Jarvis, A., Reuter, H.I., Nelson, A., Guevara, E., 2008. Hole-filled Seamless SRTM Data V4, International Centre for Tropical Agriculture (CIAT). . available from http://srtm.csi.cgiar.org.
Jones, B., 2010. Microbes in caves: agents of calcite corrosion and precipitation. In: Pedley, H.M., Rogerson, M. (Eds.), Tufas and speleothems — unravelling the microbial and physical controls: Geological Society of London, Special Publication, 336, pp. 7–30.
Kerschner, H., 1985. Quantitative paleoclimatic inferences from lateglacial snowline, timberline and rock glacier data, Tyrolean Alps, Austria. Zeitschrift fur Gletscherkunde und Glazialgeologie 21, 363–369.
Klappacher, W., 1992. Entrische Kirche. In: Klappacher, W. (Ed.), Salzburger Höhlenbuch. Landesverein für Höhlenkunde in Salzburg, Salzburg, pp. 469–485.
Labonne, M., Hillaire-Marcel, C., Ghaleb, B., Goy, J.L., 2002. Multi-isotopic age assessment of dirty speleothem calcite: an example from Altamira Cave, Spain. Quaternary Science Reviews 21, 1099–1110.
Lead, J.R., Wilkinson, K.J., 2006. Aquatic colloids and nanoparticles: current knowledge and future trends. Environmental Chemistry 3, 159–171.
Li, H.-C., Ku, T.-H., You, C.-F., Cheng, H., Edwards, R.L., Ma, Z.-B., Tsai, W.S., Li, M.-D., 2005. $^{87}Sr/^{86}Sr$ and Sr/Ca in speleothems for paleoclimate reconstruction in Central China between 70 and 280 kyr ago. Geochimica et Cosmochimica Acta 69, 3933–3947.
Lieb, G.K., 1998. High Mountain Permafrost in the Austrian Alps (Europe). In: Lewkowicz, A.C., Allard, M. (Eds.), Collection Nordica, pp. 663–668.
Linge, H.C., Lauritzen, S.E., Baker, A., Proctor, C.J., 2001. Luminescent growth banding and a stable isotope stratigraphy in a stalagmite from Northern Norway: preliminary results for the period AD 1720 to 1000 BC. Proceedings of the 13th International Congress of Speleology.
Linge, H., Baker, A., Andersson, C., Lauritzen, S.E., 2009. Variability in luminescent lamination and initial $^{230}Th/^{232}Th$ activity ratios in a late Holocene stalagmite from northern Norway. Quaternary Geochronology 4, 181–192.
Martin-Garcia, R., Martin-Perez, A. Alonso-Zarza, A., 2011. Weathering of host rock and corrosion over speleothems in Castanar cave, Spain: an example of a complex meteoric environment. 26, 83–94.
Matsuoka, N., 2005. Temporal and spatial variations in periglacial soil movements on alpine crest slopes. Earth Surface Processes and Landforms 30, 41–58.
McManus, J.F., Oppo, D.W., Cullen, J.L., Bond, G.C., 2002. Thermohaline circulation and prolonged interglacial warmth in the north Atlantic. Quaternary Research 58, 17–21.
McMillan, E.A., Fairchild, I.J., Frisia, S., Borsato, A., McDermott, F., 2005. Annual trace element cycles in calcite–aragonite speleothems: evidence of drought in the western Mediterranean 1200–1100 yrs BP. Journal of Quaternary Sciences 20, 423–433.
Meyer, M.C., Faber, R., Spötl, C., 2006. The WinGeol Lamination Tool: new software for rapid, semi-automated analysis of laminated climate archives. The Holocene 16, 1–9.
Meyer, M.C., Spötl, C., Mangini, A., 2008. The demise of the Last Interglacial recorded in isotopically dated speleothems from the Alps. Quaternary Science Reviews 27, 476–496.
Mickler, P.J., Banner, J.L., Stern, L., Asmerom, Y., Edwards, R.L., Ito, E., 2004. Stable isotope variations in modern tropical speleothems: evaluating equilibrium vs. kinetic isotope effects. Geochimica et Cosmochimica Acta 68, 4381–4393.

Mickler, P.J., Stern, L.A., Banner, J.L., 2006. Large kinetic isotope effects in modern speleothems. Geological Society of America Bulletin 118, 65–81.
Mühlinghaus, C., Scholz, D., Mangini, A., 2009. Modelling fractionation of stable isotopes in stalagmites. Geochimica et Cosmochimica Acta. 73, 7275–7289.
Müller, U.C., Kukla, G.J., 2004. North Atlantic Current and European environments during the declining stage of the Last Interglacial. Geology 32, 1009–1012.
Niggemann, S., Mangini, A., Richter, D.K., Wurth, G., 2003. A paleoclimate record of the last 17 600 yr in stalagmites from the B7 cave, Saurland, Germany. Quaternary Science Reviews 22, 555–567.
North Greenland Ice Core Project members, 2004. High-resolution record of Northern Hemisphere climate extending into the last interglacial period. Nature 431, 147–151.
Ortega, R., Maire, R., Deves, G., Quinif, Y., 2005. High-resolution mapping of uranium and other trace elements in recrystallized aragonite–calcite speleothems from caves in the Pyrenees (France): implication for U-series dating. Earth and Planetary Science Letters 237, 911–923.
Palmer, A.N., 2007. Cave Geology. Cave Books, Dayton, U.S.A.
Patzelt, W., 1994. Holocene development of all alluvial fans and the floor of the Inn valley. Mountain Research and Development 14, 283–284.
Peer, H., Zimmer, W., 1980. Geologie der Nordrahmenzone der Hohen Tauern. Jahrbuch der Geologischen Bundesanstalt 123, 411–466.
Porter, S.C., 1977. Present and post glaciation threshold in the cascade range, Washington DC, U.S.A.: topographic and climatic controls, and paleoclimatic implications. Journal of Glaciology 18, 101–115.
Railsback, L.B., Brook, G.A., Webster, J.W., 1999. Petrology and paleoenvironmental significance of detrital sand and silt in a stalagmite from Drotsky's Cave, Botswana. Physical Geography 20, 331–347.
Richards, D.A., Dorale, J.A., 2003. Uranium-series chronology and environmental applications of speleothems. In: Bourdon, B., Henderson, G.M., Lundstron, C., Turnar, S.P. (Eds.), Reviews in Mineralogy and Geochemistry, pp. 407–460. Washington D. C.
Richter, D.R., Götte, T., Niggemann, S., Wurth, G., 2004. REE 3++ and Mn 2++ activated cathodoluminescence in lateglacial and Holocene stalagmites of central Europe: evidence for climatic processes? The Holocene 14, 759.
Romanov, D., Kaufmann, G., Dreybrodt, W., 2008. $\sigma^{13}C$ profiles along growth layers of stalagmites: comparing theoretical and experimental results. Geochimica et Cosmochimica Acta 72, 438–448.
Sasowsky, I.D., Mylroie, J., 2004. Studies of Cave Sediments: Physical and Chemical Records of Paleoclimate. Kluwer Academic / Plenum Publishers, New York. 322 p.
Schimpf, D., Kilian, R., Kronz, A., Simon, K., Spoetl, C., Woerner, G., Deininger, M., Mangini, A., 2011. The significance of chemical, isotopic, and detrital components in three coeval stalagmites from the superhumid southernmost Andes (53 degrees S) as high-resolution palaeo-climate proxies. Quaternary Science Reviews 30, 443–459.
Schulte, L., Julia, R., Oliva, M., Burjachs, F., Veit, H., Carvalho, F., 2008. Sensitivity of Alpine fluvial environments in the Swiss Alps to climate forcing during the Late Holocene. IAHS publication: sediment dynamics in changing environments: Proceedings of a Symposium Held in Christchurch, New Zealand, December 2008, 325, pp. 367–374.
Shackleton, N.J., Chapman, M., Sánchez Goni, M.F., Pailler, D., Lancelot, Y., 2002. The classic marine isotope substage 5e. Quaternary Research 58, 14–16.
Shopov, Y.Y., Ford, D.C., Schwarcz, H.P., 1994. Luminescent microbanding in speleothems: high-resolution chronology and paleoclimate. Geology 22, 407–410.
Spötl, C., Fairchild, I.J., Tooth, A.F., 2005. Speleothem deposition in a dynamically ventilated cave, Obir Caves (Austrian Alps). Evidence from modern cave air and drip water monitoring. Geochimica et Cosmochimica Acta 69, 2451–2468.
Spötl, C., Holzkämper, S., Mangini, A., 2007. The last and the penultimate interglacial as recorded by speleothems from a climatically sensitive high-elevation cave site in the Alps. In: Sirocko, F., Claussen, M., Litt, T., SanchezGoni, M.F. (Eds.), The climate of past interglacials: Developments in Quaternary Science Series, v. 7. Elsevier, pp. 471–491.
Sroubek, P., Diehl, J.F., Kadlec, J., 2007. Historical climatic record from flood sediments deposited in the interior of Spiralka Cave, Czech Republic. Palaeogeography Palaeoclimatology Palaeoecology 251, 547–562.
Tan, M., Baker, A., Genty, D., Smith, C., Esper, J., Cai, B., 2006. Applications of stalagmite laminae to paleoclimate reconstructions: comparison with dendrochronology/climatology. Quaternary Science Reviews 25, 2103–2117.
Turgeon, S., Lundberg, J., 2001. Chronology of discontinuities and petrology of speleothems as paleoclimatic indicators of the Klamath Mountains, Southwest Oregon, USA. Carbonates and Evaporites 16, 153–167.
van Husen, D., 1987. LGM and Late-Glacial fluctuations in the eastern Alps. Quaternary International 38 (39), 109–118.
van Husen, D., 2000. Geological processes during the Quaternary. Mitteilungen der Österreichischen Geologischen Gesellschaft 92, 135–156.
Veit, H., 2002. Die Alpen - Geoökologie und Landschaftsentwicklung. Ulmer, Stuttgart. 352 p.
Wang, X., Neubauer, F., 1998. Orogen-parallel strike-slip faults bordering metamorphic core complexes: the Salzach–Enns fault zone in the Eastern Alps, Austria. Journal of Structural Geology 20, 799–818.
Wang, Y., Cheng, H., Edwards, R.L., Kong, X., Shao, X., Chen, S., Wu, J., Jiang, X., Wang, X., An, Z., 2008. Millennial- and orbital-scale changes in the East Asian monsoon over the past 224,000 years. Nature 451, 1090–1093.
Wiedner, E., Scholz, D., Mangini, A., Polag, D., Mühlinghaus, C., Segl, P., 2008. Investigation of the stable isotope fractionation in speleothems with laboratory experiments. Quaternary International 187, 15–24.
Wigley, T.M.L., Brown, M.C., 1976. The physics of caves. In: Ford, T.D., Cullingford, C.H.D. (Eds.), The Science of Speleology. Academic Press, London, pp. 329–358.
Zhou, H., Chi, B., Lawrence, M., Zhao, J., Yan, J., Greig, A., Feng, Y., 2008. High-resolution and precisely dated record of weathering and hydrological dynamics recorded by manganese and rare-earth elements in a stalagmite from Central. Quaternary Research 69, 438–446.